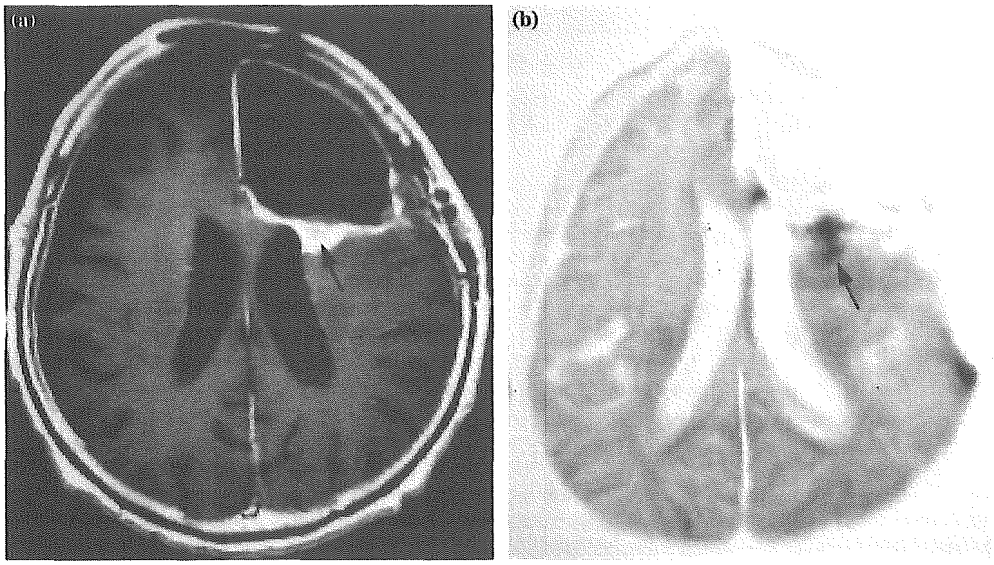

Figure 4. Conventional MRI and 3DAC of Case 7 at recurrence. (a) Gd-T1WI shows markedly enhanced mass suggesting recurrent glioblastoma in the anterior corona radiata, corresponding to the slightly darkened area in Figure 3C (arrow). (b) Recurrent glioblastoma shown as enhancement on Gd-T1WI appears black on 3DAC (arrow).

differences were found in Group A, B or D, whereas FA value was significantly lower for the responsible tract than for the non-pathological tract in Group C (Table 3).

Estimations of hemiparesis

Degree of preoperative hemiparesis varied from stage 4 to 5 in Group A, stage 2 to 5 in Group B, stage 3 to 5 in Group C and stage 1 to 5 in Group D (Table 1). Although hemiparesis before surgery tended to be more likely to be mild in Group A than in the other groups, no significant differences were identified between groups when hemiparesis was compared using the Kruskal–Wallis test ($P = 0.5$). In addition, no significant differences in postoperative hemiparesis among the four groups were identified using the Kruskal–Wallis test ($P = 0.07$). When limited to 12 patients who underwent either total or subtotal removal, improvement of hemiparesis after surgery was seen in two of the four patients in Group A, one of the three patients in Group B and all two patients in Group D. Hemiparesis did not deteriorate in any patient after surgery in these three groups. In contrast, no patients in Group C experienced improved hemiparesis after surgical intervention, and deterioration was observed in two of the three patients. Nevertheless, no significant differences in frequency of improvement were identified among the four groups using the χ^2 test for independence ($P = 0.16$). In the same 12 patients mentioned above, degree of hemiparesis before and after surgery was compared between seven patients in Group A or B and three patients in Group C, using the Mann–Whitney *U*-test. No significant difference in degree of hemiparesis before surgery was identified between Group A /B and Group C

Table 3: Comparison of FA values between non-pathological and responsible tracts for each group

Group	FA value (mean ± SD)		
	Non-pathological tract	Responsible tract	*P*
A	0.66 ± 0.08	0.63 ± 0.08	0.09
B	0.63 ± 0.09	0.55 ± 0.13	0.14
C	0.64 ± 0.11	0.34 ± 0.17	0.01
D	0.63 ± 0.20	0.50 ± 0.05	0.42

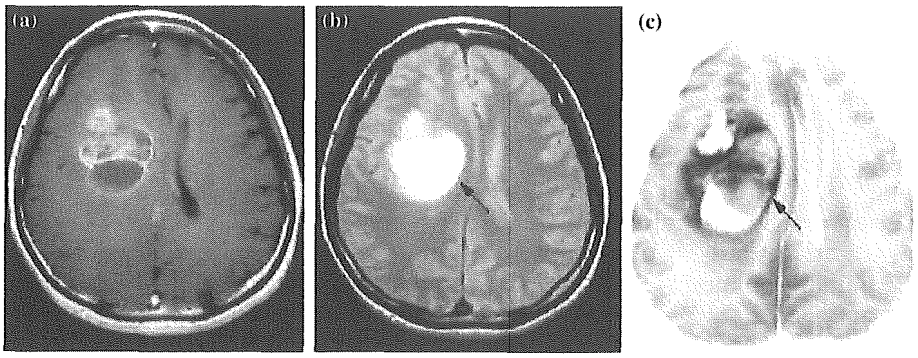

Figure 5. MR images and 3DAC in Case 18. (A) Gd-T1WI shows a huge glioblastoma in the right frontal lobe. Neither PDWI (B) nor 3DAC (C) revealthe corona radiata, due to the presence of a huge tumor. Whether the corona radiata was not apparent due to heavy compression or invasion of tumor bulk was unclear.

($P = 0.7$), while degree of hemiparesis after surgery in Group A/B was significantly milder than in Group C ($P = 0.02$).

Discussion

In the present study, 3DAC allowed clear depiction of the pyramidal tracts of the non-pathological side in all patients. These findings confirm previous reports that 3DAC offers a reliable technique for visualizing the pyramidal tracts [18,20]. The 3DAC demonstrated various findings in responsible pyramidal tracts. When PDWI clearly showed the responsible tracts without hyperintense foci, 3DAC findings also demonstrated fine detail of the responsible tracts without any change in color, as with Case 17 in Group A (Figure 1a–c). Furthermore, all patients in Group A presented with mild preoperative hemiparesis of stage 4 or 5, although no significant difference between degree of preoperative hemiparesis in Group A and the other groups was noted. When symptoms appear due to expansion of glioma, the more malignant peripheral areas of the tumor invade into dense fibers, such as the pyramidal tract. The tumor initially grows faster in one direction, as a result of fiber density, and disrupts the fibers in the next stage [29]. Results of PDWI, 3DAC and degree of hemiparesis suggest that pyramidal tracts in Group A patients did not appear to be disrupted by tumor, even if invasion to the pyramidal tract had occurred. The finding that mean FA value of the responsible tract for Group A did not differ significantly from that of the contralateral side might support this possibility that the tract is not disrupted (Table 3). Thus, 3DAC might not offer any advantages for evaluating condition of the pyramidal tract in patients for whom the responsible tract can be clearly visualized on PDWI.

When PDWI showed hyperintense foci in the responsible pyramidal tract, 3DAC demonstrated the responsible tract either as showing no change of color compared with the contralateral side, such as Case 10 in Group B (Figure 2c), or as showing darkness, like Case 7 in Group C (Figure 3c). Findings of obscured, dark areas in the pyramidal tract on 3DAC have been observed in patients with cerebral infarction. Cytotoxic edema, axonal swelling and Wallerian degeneration, all of which are seen in ischemic lesions and diffuse axonal injuries [30–32], have been suggested as hindering water diffusion, thereby creating darkened areas in the pyramidal tract on 3DAC [20,33]. In contrast, most edema surrounding a tumor, which predominantly comprises extracellular edema, should isotropically accelerate water diffusion, as extracellular edema leads to increased amounts of interstitial water [34,35]. The present study suggests that widespread hyperintense foci surrounding a tumor on PDWI result from extracellular edema rather than tumor invasion, as either no or only faint color change was apparent on 3DAC (Figures 2c and 3c, arrowheads). High cellular and/or nuclear densities have been recognized a factor hindering water diffusion [36–38]. In fact, tumor bulks displaying high cellular density are shown as areas of darkness on 3DAC in the present study. Conversely, we believe that darkened regions in the responsible tract of patients with glioblastoma resulted from a large obstruction to water diffusion due to invasion by tumor cells. Mean FA of the responsible tract for Group C was significantly decreased from that of the non-pathological side (Table 3). This finding does not directly indicate high cellular density, but suggests that the responsible tract has been largely destroyed by tumor invasion. As shown in Case 7, a dark lesion progressed on 3DAC, corresponding to a finely enhanced recurrent mass on Gd-T1WI (Figure 4a, b). This observation might also support our hypothesis that a darkened area on 3DAC is induced by tumor invasion. Furthermore, this finding suggests that 3DAC can predict infiltration of tumor cells into the pyramidal tract earlier than Gd-T1WI can. However, the responsible tract in Group B patients displayed coloration without darkness on 3DAC. No significant difference in mean FA existed between the responsible and non-pathological tracts, although mean FA of the responsible tract tended to be slightly lower than that of the non-pathological tract (Table 3). These findings suggest that the responsible tract in Group B patients was not heavily invaded or destroyed by tumor, unlike Group C. The finding of improved hemiparesis after mass reduction in one patient in Group B, compared to no patients in Group C, might support our speculation. If a hyperintense focus surrounding glioblastoma spreads to the pyramidal tract in conventional MRI on patients with hemiparesis, clinicians would hesitate over whether the pyramidal tract has been disrupted by tumor invasion. Degree of hemiparesis might not offer a predictor of pyramidal tract condition, because degree of hemiparesis before surgery did not differ significantly among the four groups. We believe that 3DAC may prove useful for examining hyperintense foci surrounding glioblastoma that have spread to the pyramidal tract on PDWI.

In Group D, we were unable to speculate on the condition of the responsible tract, as the tract was absent on 3DAC. FA value and improvement of hemiparesis after a mass reduction may lead to the speculation that the responsible tracts in Group D patients have not been largely destroyed by tumor invasion. However, 3DAC does not offer a predictor of pyramidal tract condition when the tract is not observed such as in Group D.

The present study is limited with regard to interpretations of 3DAC images. We did not undertake histological observations of responsible pyramidal tracts, and thus the amount of tumor cell invasion required for the responsible tract to become abnormally dark as in Group C remains unclear. If we assume that the responsible tracts of both Groups A and B were invaded by tumor cells, a greater degree of invasion may be present in Group B than in Group A, as PDWI revealed hyperintense foci in Group B. Again, the real differences causing these varying results remain unclear. Histological investigations into correlations between degrees of

cellular density, fiver destruction, hyperintensity on PDWI and color on 3DAC are warranted.

Conclusion

No previous reports have revealed that 3DAC findings allow suggestions as to the status of the pyramidal tract adjacent to glioblastoma. Our findings suggest that 3DAC imaging is useful for evaluating condition of the pyramidal tract, in terms of potential extensive destruction by tumor invasion, when hyperintense foci surrounding the tumor spread to the pyramidal tract on conventional MRI for glioblastoma patients with hemiparesis. Use of 3DAC with DWI will likely offer a feasible option for preoperative examination in glioblastoma patients.

Acknowledgements

This study was supported in part by the Advanced Medical Science Center, Iwate Medical University.

References

1. Gallen CC, Sobel DF, Waltz T, Aung M, Copeland B, Schwartz BJ, Hirschkoff EC, Bloom FE. Noninvasive presurgical neuromagnetic mapping of somatosensory cortex. Neurosurgery 33: 260–268, 1993
2. Atlas SW, Howard RS 2nd, Maldjian J, Alsop D, Detre JA, Listerud J, D'Esposito M, Judy KD, Zager E, Stecker M: Functional magnetic resonance imaging of regional brain activity in patients with intracerebral gliomas: findings and implications for clinical management. Neurosurgery 38: 329–338, 1996
3. Cosgrove GR, Buchbinder BR, Jiang H: Functional magnetic resonance imaging for intracranial navigation. Neurosurg Clin N Am 7: 313–322, 1996
4. Berger MS, Rostomily RC: Low grade gliomas functional mapping resection strategies, extent of resection, and outcome. J Neuro-Oncol 34: 85–101, 1997
5. Nakasato N, Kumabe T, Kanno A, Ohtomo S, Mizoi K, Yoshimoto T: Neuromagnetic evaluation of cortical auditory function in patients with temporal lobe tumors. J Neurosurg 86: 610–618, 1997
6. Karibe H, Shimizu H, Tominaga T, Koshu K, Yoshimoto T: Diffusion-weighted magnetic resonance imaging in the early evaluation of corticospinal tract injury to predict functional motor outcome in patients with deep intracerebral hemorrhage. J Neurosurg 92: 58–63, 2000
7. Krings T, Reinges MH, Thiex R, Gilsbach JM, Thron A: Functional and diffusion-weighted magnetic resonance images of space-occupying lesions affecting the motor system: imaging the motor cortex and pyramidal tracts. J Neurosurg 95: 816–824, 2001
8. Cooper RL, Chang DB, Young AC, Martin CJ, Ancker-Johnson D: Restricted diffusion in biophysical systems. Experiment Biophys J 14: 161–177, 1974
9. Le Bihan D: Diffusion, perfusion and functional magnetic resonance imaging. J Mal Vasc 20: 203–214, 1995
10. Schaefer PW, Grant PE, Gonzalez RG: Diffusion-weighted MR imaging of the brain. Radiology 217: 331–345, 2000
11. Aoyama H, Kamada K, Shirato H, Takeuchi F, Kuriki S, Iwasaki Y, Miyasaka K: Visualization of the corticospinal tract pathway using magnetic resonance axonography and magnetoencephalography for stereotactic irradiation planning of arteriovenous malformations. Radiother Oncol 68: 27–32, 2003
12. Holodny AI, Schwartz TH, Ollenschleger M, Liu WC, Schulder M: Tumor involvement of the corticospinal tract: diffusion magnetic resonance tractography with intraoperative correlation. J Neurosurg 95: 1082, 2001
13. Parmar H, Sitoh YY, Yeo TT: Combined magnetic resonance tractography and functional magnetic resonance imaging in evaluation of brain tumors involving the motor system. J Comput Assist Tomogr 28: 551–556, 2004
14. Watanabe T, Honda Y, Fujii Y, Koyama M, Matsuzawa H, Tanaka R: Three-dimensional anisotropy contrast magnetic resonance axonography to predict the prognosis for motor function in patients suffering from stroke. J Neurosurg 94: 955–960, 2001
15. Watanabe T, Honda Y, Fujii Y, Koyama M, Tanaka R: Serial evaluation of axonal function in patients with brain death by using anisotropic diffusion-weighted magnetic resonance imaging. J Neurosurg 56–60, 2004
16. Witwer BP, Moftakhar R, Hasan KM, Deshmukh P, Haughton V, Field A, Arfanakis K, Noyes J, Moritz CH, Meyerand ME, Rowley HA, Alexander AL, Badie B: Diffusion-tensor imaging of white matter tracts in patients with cerebral neoplasm. J Neurosurg 97: 568–575, 2002
17. Nakada T, Matsuzawa H, Kwee IL: Magnetic resonance axonography of the rat spinal cord. Neuroreport 27: 2053–2056, 1994
18. Nakada T, Nakayama N, Fujii Y, Kwee IL: Clinical application of three-dimensional anisotropy contrast magnetic resonance axonography. Technical note. J Neurosurg 90: 791–795, 1999
19. Inoue T, Shimizu H, Yoshimoto T: Imaging the pyramidal tract in patients with brain tumors. Clin Neurol Neurosurg 101: 4–10, 1999
20. Inoue T, Shimizu H, Yoshimoto T, Kabasawa H: Spatial functional distribution in the corticospinal tract at the corona radiata: a three-dimensional anisotropy contrast study. Neurol Med Chir 41: 293–299, 2001
21. Coenen VA, Krings T, Mayfrank L, Polin RS, Reinges MH, Thron A, Gilsbach JM: Three-dimensional visualization of the pyramidal tract in a neuronavigation system during brain tumor surgery: first experiences and technical note. Neurosurgery 49: 86–93, 2001
22. Holodny AI, Schwartz TH, Ollenschleger M, Liu WC, Schulder M: Tumor involvement of the corticospinal tract: diffusion magnetic resonance tractography with intraoperative correlation. J Neurosurg 95: 1082, 2001
23. Kamada K, Houkin K, Iwasaki Y, Takeuchi F, Kuriki S, Mitsumori K, Sawamura Y: Rapid identification of the primary motor area by using magnetic resonance axonography. J Neurosurg 97: 558–567, 2002
24. Kashimura H, Inoue T, Ogasawara K, Ogawa: Preoperative evaluation of neural tracts by use of three-dimensional anisotropy contrast imaging in a patient with brainstem cavernous angioma: technical case report. Neurosurgery 52: 1226–1230, 2003
25. Darwin RH, Drayer BP, Riederer SJ, Wang HZ, MacFall JR: T2 estimates in healthy and diseased brain tissue: a comparison using various MR pulse sequences. Radiology 160: 375–381, 1986
26. Papadakis NG, Xing D, Houston GC, Smith JM, Smith MI, James MF, Parsons AA, Huang CL, Hall LD, Carpenter TA: A study of rotationally invariant and symmetric indices of diffusion anisotropy. Magn Reson Imaging 17(6): 881–892, 1999
27. Sorensen AG, Wu O, Copen WA, Davis TL, Gonzalez RG, Koroshetz WJ, Reese TG, Rosen BR, Wedeen VJ, Weisskoff RM: Human acute cerebral ischemia: detection of changes in water diffusion anisotropy by using MR imaging. Radiology 212(3): 785–792, 1999
28. Brunnstrom S: Motor testing procedures in hemiplegia. J APTA 46: 357–375, 1966
29. Yasargil MG: Microneurosurgery IV A (In 4 volumes). Georg Thieme, Stuttgart/New York Verlag (for distribution in Japan: Nankodo Company, Tokyo), 1993, pp. 127–134
30. Barzo P, Marmarou A, Fatouros P, Hayasaki K, Corwin F: Contribution of vasogenic and cellular edema to traumatic brain

swelling measured by diffusion-weighted imaging. J Neurosurg 87: 900–907, 1997
31. Castillo M, Mukherji SK. Early abnormalities related to postinfarction Wallerian degeneration: evaluation with MR diffusion-weighted imaging. J Comput Assist Tomogr 23: 1004–1007, 1999
32. Mukherjee P, Bahn MM, McKinstry RC, Shimony JS, Cull TS, Akbudak E, Snyder AZ, Conturo TE: Differences between gray matter and white matter water diffusion in stroke: diffusion-tensor MR imaging in 12 patients. Radiology 215: 211–220, 2000
33. Igarashi H, Katayama Y, Tsuganezawa T, Yamamuro M, Terashi A, Owan C: Three-dimensional anisotropy contrast (3DAC) magnetic resonance imaging of the human brain: application to assess Wallerian degeneration. Intern Med 37: 662–668, 1998
34. Gonatas NK, Zimmerman HM, Levine S: Ultrastructure of inflammation with edema in the rat brain. Am J Pathol 42: 455–469, 1963
35. Schwartz RB, Mulkern RV, Gudbjartsson H, Jolesz F. Diffusion-weighted MR imaging in hypertensive encephalopathy: clues to pathogenesis. AJNR Am J Neuroradiol 19: 859–862, 1998
36. Sugahara T, Korogi Y, Kochi M, Ikushima I, Shigematu Y, Hirai T, Okuda T, Liang L, Ge Y, Komohara Y, Ushio Y, Takahashi M: Usefulness of diffusion-weighted MRI with echo-planar technique in the evaluation of cellularity in gliomas. J Magn Reson Imaging 9: 53–60, 1999
37. Okamoto K, Ito J, Ishikawa K, Sakai K, Tokiguchi S: Diffusion-weighted echo-planar MR imaging in differential diagnosis of brain tumors and tumor-like conditions. Eur Radiol 10: 1342–1350, 2000
38. Gauvain KM, McKinstry RC, Mukherjee P, Perry A, Neil JJ, Kaufman BA, Hayashi RJ. Evaluating pediatric brain tumor cellularity with diffusion-tensor imaging. AJR Am J Roentgenol 177: 449–454, 2002

Address for offprints: Takaaki Beppu, Department of Neurosurgery, Iwate Medical University, 19—1, Uchimaru, Morioka 020—8505, Japan; Tel.: 019-651-5111; Fax: 019-625-8799; E-mail: tbeppu@iwate-med.ac.jp

ELSEVIER

Clinical Neurology and Neurosurgery 107 (2005) 174–180

Clinical Neurology and Neurosurgery

www.elsevier.com/locate/clineuro

Diffusion tensor imaging for preoperative evaluation of tumor grade in gliomas

Takashi Inoue[a,*], Kuniaki Ogasawara[a], Takaaki Beppu[a], Akira Ogawa[a], Hiroyuki Kabasawa[b]

[a] *Department of Neurosurgery, Iwate Medical University School of Medicine, 19-1 Uchimaru, Morioka, Iwate 020-8505, Japan*
[b] *GE Yokogawa Medical Systems, Tokyo, Japan*

Received 15 September 2003; received in revised form 24 May 2004; accepted 8 June 2004

Abstract

The relationship between water diffusion parameters measured using diffusion tensor imaging (DTI) and histological malignancy of gliomas was investigated.

DTI was performed using a 3.0 T MR scanner in 41 consecutive patients with histologically proven gliomas. Fractional anisotropy (FA) and mean diffusivity (MD) were calculated and compared with the WHO classification of the gliomas.

The FA values of grade 1 gliomas (0.150 ± 0.017) were significantly lower than those of grade 3 (0.23 ± 0.033) or grade 4 gliomas (0.229 ± 0.033) ($P < 0.0001$, respectively). The FA values of grade 2 gliomas (0.159 ± 0.018) were significantly lower than those of grade 3 or grade 4 gliomas ($P = 0.0002$, $P < 0.0001$, respectively). The FA threshold between low grade and high grade gliomas was 0.188. The MD values of grade 1 gliomas (1619.1 ± 157.4 × 10^{-6} mm^2/s) were significantly higher than those of grade 3 (1084.5 ± 218.9 × 10^{-6} mm^2/s) ($P = 0.0036$) or grade 4 gliomas (1098.0 ± 291.6 × 10^{-6} mm^2/s) ($P = 0.0002$). The MD values were not correlated with the other grades of glioma.

FA values can distinguish between high grade and low grade gliomas. This is useful in deciding the surgical strategy or selecting the site of stereotactic biopsy.

Keywords: Diffusion tensor imaging; Glioma; Malignancy

1. Introduction

Gliomas are the most common primary neoplasms of the central nervous system [1]. The prognosis for patients with high grade gliomas has remained poor despite improvements in radiation and chemotherapy [2,3]. Accurate preoperative diagnosis of the tumor grade is important for the determination of appropriate treatment strategies [4]. Magnetic resonance (MR) spectroscopy [5–8], single photon emission computed tomography [9–13], or positron emission tomography [9–11] have all been used for the preoperative evaluation of glioma malignancy. However, MR spectroscopy has limitations in spatial resolution and heterogeneous lesions are difficult to assess [7], whereas imaging methods using radioactive isotopes are invasive and involve handling problems.

Diffusion tensor imaging (DTI) can measure the directionality (anisotropy) and the magnitude (diffusivity) of water diffusion in vivo [14]. Fractional anisotropy (FA) and mean diffusivity (MD) are the quantitative indices for anisotropy and diffusivity, respectively [15]. The microstructural organization of the brain tissue affects the molecular motion of water. Therefore, the FA and MD reflect microstructural changes of tissue caused by damage from degenerative disease, brain ischemia and brain tumors [16–21]. The histological diagnosis of glioma malignancy is based on the presence of nuclear heteromorphism, nuclear mitosis, endothelial proliferation, and necrosis [22]. These characteristics may affect the FA and MD values of gliomas.

* Corresponding author. Tel.: +81 19 651 5111; fax: +81 19 625 8799.
E-mail address: tainoue@iwate-med.ac.jp (T. Inoue).

0303-8467/$ – see front matter © 2004 Elsevier B.V. All rights reserved.
doi:10.1016/j.clineuro.2004.06.011

Table 1
Patient characteristics and tumor grades, using the WHO classification

Case no.	Age	Sex	Grade	FA value	MD value × 10^{-6} mm^2/s
1	7	F	G1	0.161	1552.6
2	10	F	G1	0.140	1395.9
3	15	F	G1	0.152	1706.3
4	23	F	G1	0.165	1525.9
5	6	M	G1	0.150	1779.7
6	27	M	G1	0.154	1448.7
7	43	M	G1	0.112	1797.73
8	69	M	G1	0.163	1745.91
9	35	F	G2	0.158	1087.9
10	46	F	G2	0.172	1010.1
11	48	F	G2	0.144	969.9
12	2	M	G2	0.176	1588.0
13	28	M	G2	0.154	1403.2
14	33	M	G2	0.163	1251.3
15	40	M	G2	0.122	1380.94
16	59	M	G2	0.181	1407.37
17	60	M	G2	0.157	1493.2
18	43	F	G3	0.231	1328.5
19	68	F	G3	0.237	778.8
20	4	M	G3	0.227	951.9
21	39	M	G3	0.206	1270.26
22	51	M	G3	0.203	957.3
23	60	M	G3	0.293	1220.12
24	41	F	G4	0.214	877.7
25	44	F	G4	0.195	1085.8
26	54	F	G4	0.199	972.11
27	58	F	G4	0.250	874.3
28	68	F	G4	0.218	612.7
29	68	F	G4	0.207	1146.8
30	68	F	G4	0.319	1385.69
31	69	F	G4	0.196	1278.4
32	77	F	G4	0.220	1224.8
33	15	M	G4	0.219	694.7
34	47	M	G4	0.225	865.2
35	56	M	G4	0.216	1328.77
36	61	M	G4	0.212	1326.9
37	63	M	G4	0.283	875.67
38	63	M	G4	0.232	1049.6
39	64	M	G4	0.204	1838.47
40	72	M	G4	0.257	1286.71
41	74	M	G4	0.251	1038.82

This study evaluates the relationship between the findings of DTI and the histological malignancy of gliomas.

2. Clinical material and methods

2.1. Patient population

This study included 41 consecutive patients (18 females and 23 males) aged 2–77 years (mean 46 years) treated at our institute between October 2000 and December 2002, who underwent DTI and had a histological diagnosis. No medical therapy was received for their tumor prior to imaging. The patient characteristics and tumor grades, using the WHO classification [23], are listed in Table 1. The study protocol was approved by the local ethical committee. All subjects gave written informed consent prior to the study.

2.2. MR imaging

All MR imaging used a Signa VH/i 3.0 T MR imaging system (General Electric Medical Systems, Milwaukee, WI) and standard head coil. A spin echo echo planar imaging (EPI) sequence with diffusion gradients applied in six directions ((x, y, z): (101), (−101), (011), (01 −1), (110) and (−110) direction, respectivery) was used for DTI: repetition time 10,000 ms, echo time 84 ms, matrix 256 × 260, field of view 240 mm, number of excitations 6, slice thickness 6 mm, gap 2 mm, and b factor 800 s/mm^2. All patients underwent conventional spin echo T1-weighted imaging with contrast medium after DTI.

2.3. Image analysis

All image post processing was performed on a scanner console using a subprogram, developed by one of the authors (H.K.), of the Functool™ image analysis software (General Electric Medical Systems, Buc, France). The scalars invariants of the tensor, FA and MD, were derived for every pixel. The regions of interest (ROIs) were determined on the T2-weighted EPI scans, and were positioned on the solid portion of the lesions. In the enhanced tumors, the ROIs were confirmed to set the enhanced lesion on the T1 weighted images with contrast medium. The ROIs were automatically transferred onto the coregistered FA and MD maps (Fig. 1). Then, the FA and MD values were calculated for each patient.

2.4. Statistical analysis

The relationship between the FA or MD values and the tumor grade was evaluated with Scheffe's F test. Statistical significance was set at $P < 0.05$.

3. Results

DTI demonstrated the tumor mass and cystic lesions in all patients. Representative FA maps and T1-weighted images with contrast medium are shown in Fig. 2. The relationships between the FA or MD values and the tumor grade are shown in Figs. 3 and 4, respectively.

The FA values of grade 1 gliomas (0.150 ± 0.017) were significantly lower than those of grade 3 (0.23 ± 0.033) or grade 4 gliomas (0.229 ± 0.033) ($P < 0.0001$, respectively). The FA values of grade 2 gliomas (0.159 ± 0.018) were significantly lower than those of grade 3 or grade 4 gliomas ($P = 0.0002$, $P < 0.0001$, respectively). The FA threshold between low grade (grade 1 and 2) and high grade gliomas (grade 3 and 4) was 0.188 (Fig. 3). Differences between the

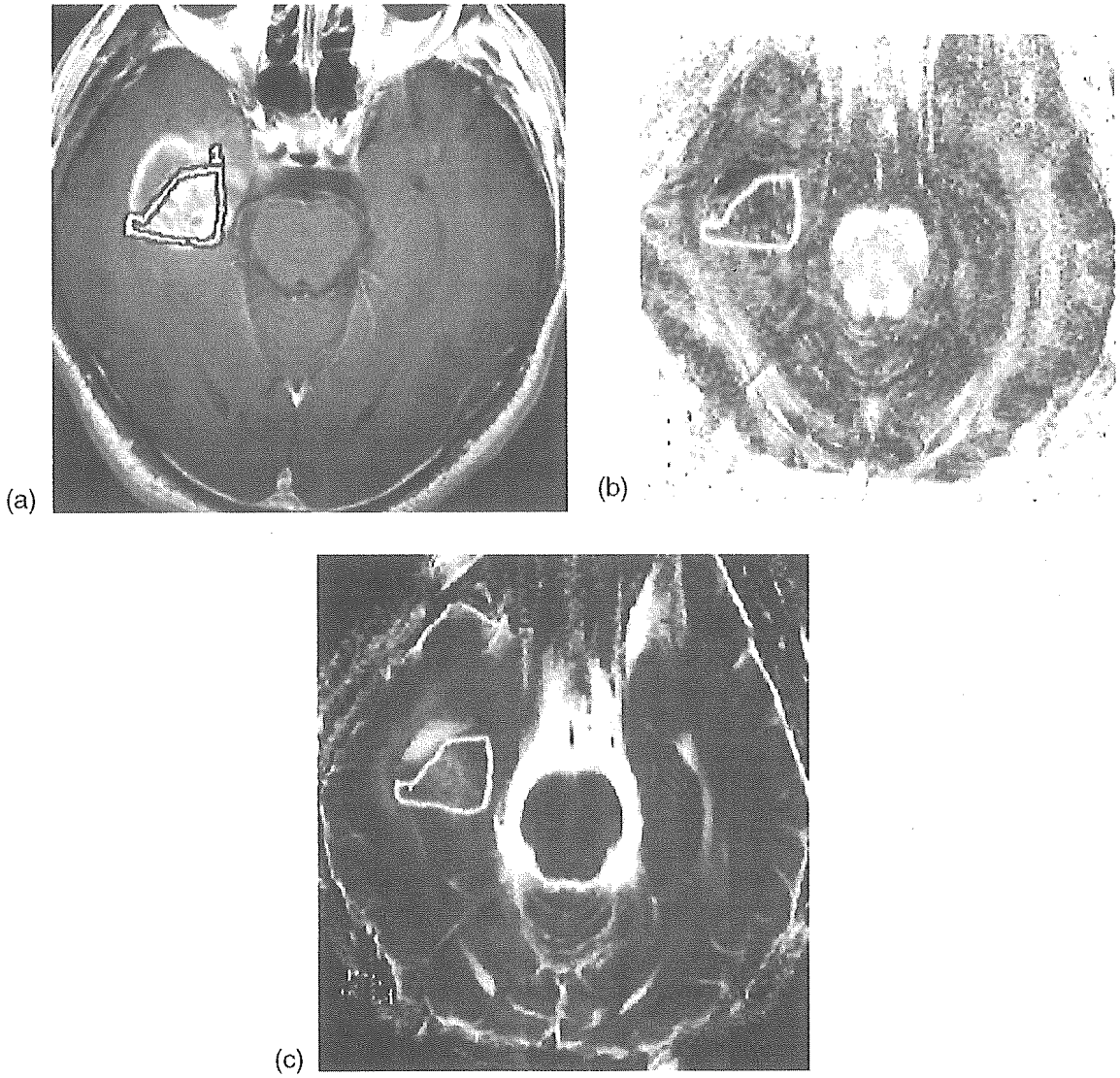

Fig. 1. (a) T1-weighted magnetic resonance (MR) image with contrast medium showing the region of interest (ROI) in the solid portion of the lesion. (b) Fractional anisotropy map showing the outline of the ROI traced automatically. (c) Mean diffusivity map showing the outline of the ROI traced automatically.

FA values of grades 1 and 2, or grades 3 and 4 were not significant.

The MD values of grade 1 gliomas ($1619.1 \pm 157.4 \times 10^{-6}$ mm^2/s) were significantly higher than those of grade 3 ($1084.5 \pm 218.9 \times 10^{-6}$ mm^2/s) ($P = 0.0036$) or grade 4 gliomas ($1098.0 \pm 291.6 \times 10^{-6}$ mm^2/s) ($P = 0.0002$). Differences between the MD values of grade 1 and 2 ($1288.0 \pm 220.2 \times 10^{-6}$ mm^2/s), 2 and 3, and 3 and 4 were not significant. There was no clear threshold value between low grade and high grade gliomas (Fig. 4).

4. Discussion

The primary finding of the present study was that the FA value could be used to distinguish high grade glioma from low grade glioma.

FA values have been investigated in patients with multiple sclerosis, amyotrophic lateral sclerosis, or leukoaraiosis, showing that the FA value is an indicator of the tissue damage of white matter [17–20,24]. The molecular movement of water is restricted by membranes in the brain [25]. The presence of myelinated fibers is an important factor in the underlying mechanisms of anisotropic diffusion [26]. Thus, damaged tissue in myelinated fibers may have reduced FA values. Anisotropy is always reduced in brain tumors [21]. In the present study, the FA values of gliomas were lower than those of subcortical white (0.76 ± 0.05) and gray (0.25 ± 0.1) matter [21], which corresponded with previous findings.

The present study showed that the FA values of high grade gliomas were significantly higher than those of low grade gliomas. High anisotropy implies that the tissue is symmetrically organized [21]. High grade glioma is histologically characterized by pseudo-palisading, endothelial

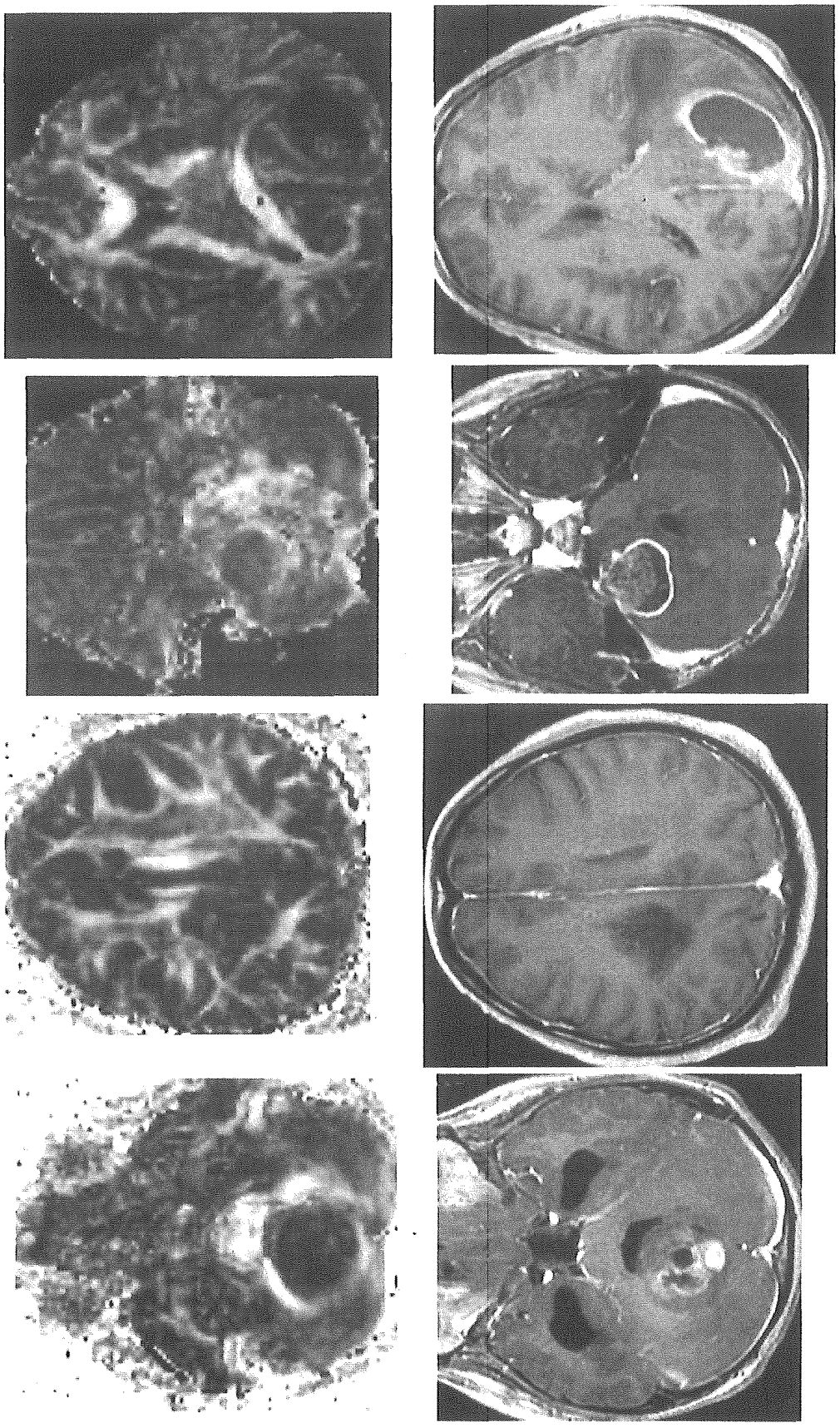

Fig. 2. Representative fractional anisotropy maps (upper row) and T1-weighted MR images with contrast medium (lower row).

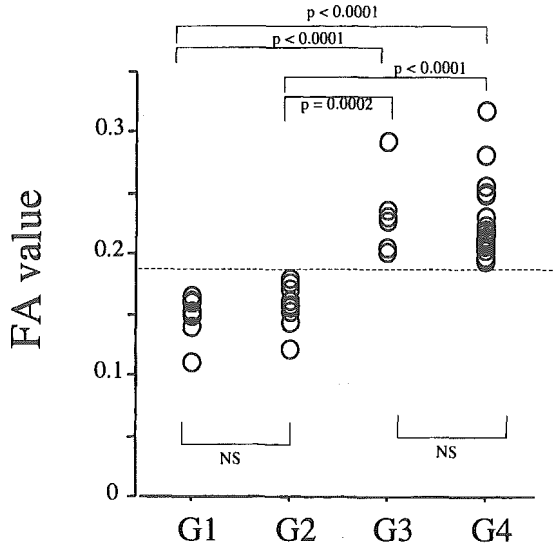

Fig. 3. Fractional anisotropy (FA) values and glioma grade. Dashed line, threshold between low grade (G1 and G2) and high grade gliomas (G3 and G4).

proliferation, or glomerular formation. The symmetric histological organization may influence the anisotropy and increase the FA value. However, high grade glioma is also characterized by necrosis. Actually, it was reported that the necrotic core of the high grade gliomas showed low FA values [27]. Therefore, in the present study we strictly limited the ROIs to be within the tumor body and to avoid the inclusion of large necrosis. Thus, our findings suggest that preoperative measurement of the FA values may predict the malignancy of gliomas, which may be useful in deciding the surgical strategy or selecting the site of stereotactic biopsy.

In the present study, the MD values of grade 1 gliomas were significantly higher than those of high grade gliomas.

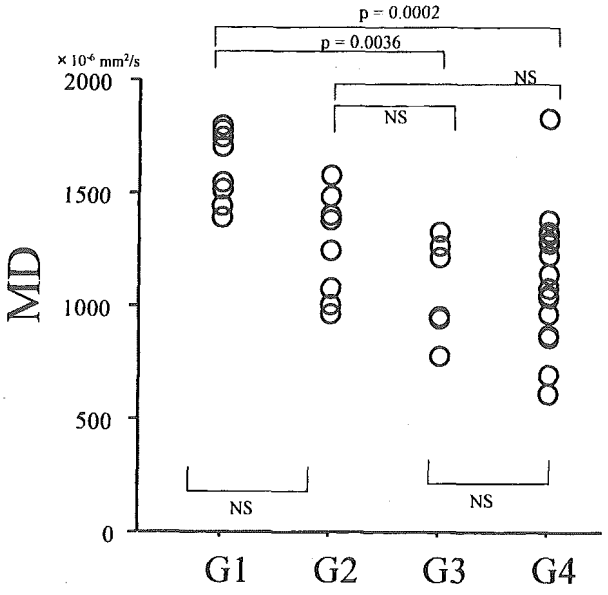

Fig. 4. Mean diffusivity (MD) values and glioma grade.

However, the other grades of glioma did not correlate with the MD values. Thus, the MD value was a poor predictor to distinguish the malignancy of gliomas in comparison with the FA value. MD values have been correlated with the histological cellularity of gliomas and are useful to distinguish low grade gliomas from high grade gliomas [4]. The exact reason for this discrepancy between previous findings and our results is difficult to assess, but there are several possible explanations. First, microstructural changes including cell swelling, shrinkage, or widening of the extracellular space can affect the MD values [28,29]. Second, low grade glioma may exhibit moderate or high cellularity [30,31]. Thus, the MD values may not correlate with the glioma grades.

Cystic changes or necrosis within lesions could decrease or increase FA and MD values, respectively. Therefore, we excluded that possibility by using high resolution DTI. High field MR imaging is useful to investigate fine anatomical structures [32,33], so cyst or necrosis within the tumor is easily differentiated from the solid portion.

Our study has some limitations regarding interpretation of the FA values. First is the normal variation in the FA values among different brain regions. For example, there is a more than 2-fold difference in the FA values between peripheral white matter such as neocortical association tracts and central commissural tracts such as the splenium of the corpus callosum [34,35]. If high grade gliomas tend to occur in deep white matter, they may have higher FA value. In fact, "butterfly gliomas" found at the splenium of the corpus callosum tend to be Grade IV glioma rather than Grade I or II gliomas. Second is the heterogeneity of the FA and the MD values within tumors. Although this may not cause serious problems in entirely homogenous tumors, discrepancy may have occurred between the ROIs and histologic samples in heterogeneous tumors. An image-guided technique, which was not applied in the present study for the purpose of tissue sampling, would improve spatial correlation between the samples examined by DTI and histologic examination. Third is that DTI did not cancel the perfusion effects. Tumor vascularity or microcirculation in the pathological tissue may affect the FA values. We should apply higher b value DTI to reduce the contribution of the perfusion effects [36–38]. However, higher b value DTI reduces the signal to noise ratio instead of reduction of the contribution of the perfusion effects. In our study, we used high resolution DTI to set the ROIs in the tumor bulk, not in the cystic or necrotic regions. Therefore, we used b value of 800 s/mm^2 in this investigation. Further investigation to compare the findings of DTI and histological examination is required.

5. Conclusion

Investigation of the relationship between DTI and histological malignancy of gliomas found that the FA value can

distinguish high grade glioma from low grade glioma. This may be useful in deciding the surgical strategy or selecting the site of stereotactic biopsy.

Acknowledgement

This work was supported in part by Grants-in-Aid for Advanced Medical Science Research by the Ministry of Education, Culture, Sports, Science, and Technology, Japan.

References

[1] Russell D, Rubinstein L. Tumours of central neuroepithelial origin. In: Rubinstein L, editor. Pathology of tumours of the nervous system. Baltimore: Williams & Wilkins; 1989. p. 83–350.
[2] Kayama T, Kumabe T, Tominaga T, Yoshimoto T. Prognostic value of complete response after the initial treatment for malignant astrocytoma. Neurol Res 1996;18:321–4.
[3] Black PM. Brain tumors. Part 1. N Engl J Med 1991;324:1471–6.
[4] Sugahara T, Korogi Y, Kochi M, Ikushima I, Shigematu Y, Hirai T, et al. Usefulness of diffusion-weighted MRI with echo-planar technique in the evaluation of cellularity in gliomas. J Magn Reson Imaging 1999;9:53–60.
[5] Burtscher IM, Stahlberg F, Holtas S. Proton (1H) MR spectroscopy for routine diagnostic evaluation of brain lesions. Acta Radiol 1997;38:953–60.
[6] Shimizu H, Kumabe T, Tominaga T, Kayama T, Hara K, Ono Y, et al. Noninvasive evaluation of malignancy of brain tumors with proton MR spectroscopy. AJNR Am J Neuroradiol 1996;17:737–47.
[7] Shimizu H, Kumabe T, Shirane R, Yoshimoto T. Correlation between choline level measured by proton MR spectroscopy and Ki-67 labeling index in gliomas. AJNR Am J Neuroradiol 2000;21:659–65.
[8] Shukla-Dave A, Gupta RK, Roy R, Husain N, Paul L, Venkatesh SK, et al. Prospective evaluation of in vivo proton MR spectroscopy in differentiation of similar appearing intracranial cystic lesions. Magn Reson Imaging 2001;19:103–10.
[9] Sfakianakis G. Preoperative grading of gangliogliomas using FDG PET and Tl-201 SPECT: comments from a nuclear medicine view. AJNR Am J Neuroradiol 1998;19:811.
[10] Kincaid PK, El-Saden SM, Park SH, Goy BW. Cerebral gangliogliomas: preoperative grading using FDG-PET and 201Tl-SPECT. AJNR Am J Neuroradiol 1998;19:801–6.
[11] Tamura M, Shibasaki T, Zama A, Kurihara H, Horikoshi S, Ono N, et al. Assessment of malignancy of glioma by positron emission tomography with 18F-fluorodeoxyglucose and single photon emission computed tomography with thallium-201 chloride. Neuroradiology 1998;40:210–5.
[12] Kallen K, Heiling M, Andersson AM, Brun A, Holtas S, Ryding E, et al. Evaluation of malignancy in ring enhancing brain lesions on CT by thallium-201 SPECT. J Neurol Neurosurg Psychiatry 1997;63:569–74.
[13] Kumabe T, Shimizu H, Sonoda Y, Shirane R. Thallium-201 single-photon emission computed tomographic and proton magnetic resonance spectroscopic characteristics of intracranial ganglioglioma: three technical case reports. Neurosurgery 1999;45:183–7.
[14] Pierpaoli C, Basser PJ. Toward a quantitative assessment of diffusion anisotropy. Magn Reson Med 1996;36:893–906.
[15] Basser PJ, Pierpaoli C. Microstructural and physiological features of tissues elucidated by quantitative-diffusion-tensor MRI. J Magn Reson B 1996;111:209–19.
[16] Bammer R, Augustin M, Strasser-Fuchs S, Seifert T, Kapeller P, Stollberger R, et al. Magnetic resonance diffusion tensor imaging for characterizing diffuse and focal white matter abnormalities in multiple sclerosis. Magn Reson Med 2000;44:583–91.
[17] Ciccarelli O, Werring DJ, Wheeler-Kingshott CA, Barker GJ, Parker GJ, Thompson AJ, et al. Investigation of MS normal-appearing brain using diffusion tensor MRI with clinical correlations. Neurology 2001;56:926–33.
[18] Ellis CM, Simmons A, Jones DK, Bland J, Dawson JM, Horsfield MA, et al. Diffusion tensor MRI assesses corticospinal tract damage in ALS. Neurology 1999;53:1051–8.
[19] Filippi M, Cercignani M, Inglese M, Horsfield MA, Comi G. Diffusion tensor magnetic resonance imaging in multiple sclerosis. Neurology 2001;56:304–11.
[20] Tievsky AL, Ptak T, Farkas J. Investigation of apparent diffusion coefficient and diffusion tensor anisotrophy in acute and chronic multiple sclerosis lesions. AJNR Am J Neuroradiol 1999;20:1491–9.
[21] Wieshmann UC, Clark CA, Symms MR, Franconi F, Barker GJ, Shorvon SD. Reduced anisotropy of water diffusion in structural cerebral abnormalities demonstrated with diffusion tensor imaging. Magn Reson Imaging 1999;17:1269–74.
[22] Daumas-Duport C, Scheithauer B, O'Fallon J, Kelly P. Grading of astrocytomas: a simple and reproducible method. Cancer 1988;62:2152–65.
[23] Kleihues P, Sobin LH. World Health Organization classification of tumors. Cancer 2000;88:2887.
[24] Jones DK, Lythgoe D, Horsfield MA, Simmons A, Williams SC, Markus HS, et al. Characterization of white matter damage in ischemic leukoaraiosis with diffusion tensor MRI. Stroke 1999;30:393–7.
[25] Hajnal JV, Doran M, Hall AS, Collins AG, Oatridge A, Pennock JM, et al. MR imaging of anisotropically restricted diffusion of water in the nervous system: technical, anatomic, and pathologic considerations. J Comput Assist Tomogr 1991;15:1–18.
[26] Le Bihan D. Anisotropic diffusion of brain whtie matter reviseted: restrictions, permeability and tortuosity. In: Book of abstracts. Presented at ISMRM, Berkeley, CA, 1996.
[27] Sinha S, Bastin ME, Whittle IR, Wardlaw JM. Diffusion tensor MR imaging of high-grade cerebral gliomas. AJNR Am J Neuroradiol 2002;23:520–7.
[28] Sevick RJ, Kanda F, Mintorovitch J, Arieff AI, Kucharczyk J, Tsuruda JS, et al. Cytotoxic brain edema: assessment with diffusion-weighted MR imaging. Radiology 1992;185:687–90.
[29] Anderson AW, Zhong J, Petroff OA, Szafer A, Ransom BR, Prichard JW, et al. Effects of osmotically driven cell volume changes on diffusion-weighted imaging of the rat optic nerve. Magn Reson Med 1996;35:162–7.
[30] Giannini C, Scheithauer BW, Weaver AL, Burger PC, Kros JM, Mork S, et al. Oligodendrogliomas: reproducibility and prognostic value of histologic diagnosis and grading. J Neuropathol Exp Neurol 2001;60:248–62.
[31] Sato Y, Ochiai H, Yamakawa Y, Nabeshima K, Asada Y, Hayashi T, et al. Brain surface ependymoma. Neuropathology 2000;20:315–8.
[32] Harada A, Fujii Y, Yoneoka Y, Takeuchi S, Tanaka R, Nakada T, et al. High-field magnetic resonance imaging in patients with moyamoya disease. J Neurosurg 2001;94:233–7.
[33] Fujii Y, Nakayama N, Nakada T. High-resolution T2-reversed magnetic resonance imaging on a high magnetic field system: technical note. J Neurosurg 1998;89:492–5.
[34] Shimony JS, McKinstry RC, Akbudak E, Aronovitz JA, Snyder AZ, Lori NF, et al. Quantitative diffusion-tensor anisotropy brain MR imaging: normative human data and anatomic analysis. Radiology 1999;212:770–84.
[35] Pierpaoli C, Jezzard P, Basser PJ, Barnett A, Di Chiro G. Diffusion tensor MR imaging of the human brain. Radiology 1996;201:637–48.

[36] Yoshiura T, Wu O, Zaheer A, Reese TG, Sorensen AG. Highly diffusion-sensitized MRI of brain: Dissociation of gray and white matter. Magn Reson Med 2001;45:734–40.
[37] Meyer JR, Gutierrez A, Mock B, Hebron D, Prager JM, Gorey MT, et al. High-*b*-value diffusion-weighted MR imaging of suspected brain infarction. AJNR Am J Neuroradiol 2000;21:1821–9.
[38] Melhem ER, Itoh R, Jones L, Barker PB. Diffusion tensor MR imaging of the brain: effect of diffusion weighting on trace and anisotropy measurements. AJNR Am J Neuroradiol 2000;21:1813–20.

Available online at www.sciencedirect.com
SCIENCE DIRECT®
Cancer Letters 191 (2003) 109–119
CANCER Letters
www.elsevier.com/locate/canlet

Introduction of wild-type p53 enhances thrombospondin-1 expression in human glioma cells

Hironobu Harada[a,*], Kou Nakagawa[a], Masahiro Saito[a], Shohei Kohno[a], Shigeyuki Nagato[a], Koji Furukawa[a], Yoshiaki Kumon[a], Katsuyuki Hamada[b], Takanori Ohnishi[a]

[a]*Department of Neurosurgery, Ehime University School of Medicine, Shigenobu-cho, Onsen-gun, Ehime 791-0295, Japan*
[b]*Department of Obstetrics and Gynecology, Ehime University School of Medicine, Shigenobu-cho, Onsen-gun, Ehime 791-0295, Japan*

Received 26 August 2002; accepted 7 October 2002

Abstract

Malignant gliomas are distinguished from low-grade gliomas by their intense angiogenesis. In gliomas, *p53* is the most frequently altered gene and is involved in the early phase of glioma development. In contrast, homozygous *p16* gene deletion is more common in high-grade gliomas. In order to understand the mechanism by which gliomas become more angiogenic during the malignant transformation, we examined the relationship between thrombospondin-1, a negative regulator in angiogenesis, and these tumor suppressor genes in malignant gliomas. Human glioma cell line U-251 MG, which has mutated *p53* and deleted *p16*, was transduced with recombinant replication-defective adenovirus vectors containing the cDNA of wild-type *p53*, *p16*, and *p21*. Only the induction of wild-type *p53* enhanced expression of thrombospondin-1 mRNA and the protein in U-251 MG cells. Furthermore, thrombospondin-1 that was secreted in the culture medium was significantly increased (3.8-fold) as compared with that of the viral control 36 h after infection with Ad5CMV-*p53*. In the presence of wild-type *p53* plasmid DNA, the promoter activity was increased 7.4-fold as compared with an empty expression vector control. These studies may suggest that mutation of *p53* gene endows gliomas with an angiogenic phenotype by reducing thrombospondin-1 production as well as enhancing the angiogenesis inducers in the early phase of malignant progression.

Keywords: p53; p16; Thrombospondin-1; Angiogenesis; Glioma

1. Introduction

The development of neovascularization is a prerequisite of sustaining the growth, invasion, and metastasis of tumors. The balance between stimulators and inhibitors regulates the angiogenic response, and various cytokines related to angiogenesis have been identified at the protein or transcript levels. Among the many regulators known to act on vasculature, vascular endothelial growth factor (VEGF) and basic fibroblast growth factor represent the most potent inducers of tumor angiogenesis. In contrast, thrombospondin-1 (TSP1) has been noted as a negative regulator. TSP1 is a multifunctional matrix

* Corresponding author. Tel.: +81-89-960-5338; fax: +81-89-960-5340.
E-mail address: harada@m.iheme-u.ac.jp (H. Harada).

0304-3835/02/$ - see front matter
doi:10.1016/S0304-3835(02)00592-X

glycoprotein consisting of a disulfide-bonded trimer with a molecular weight of 450 kDa, and it is secreted from fibroblasts, macrophages, and neoplastic cells. TSP1 has been demonstrated to inhibit endothelial cell adhesion, motility, and growth and to induce apoptosis in endothelial cells [1].

Malignant gliomas belong to hypervascular neoplasms, which are responsible for rapid growth and poor prognosis [2]. A multistep cascade proceeding from a non-neoplastic cell to a low-grade and finally to a high-grade malignancy has been molecularly characterized in gliomas [3]. In particular, mutations of *p53* are frequently observed and represent consistent molecular genetic alterations in low-grade gliomas. In high-grade gliomas, a high frequency of homozygous *p16* gene deletion has been demonstrated [4–6]. The cellular phenotypic changes in tumor progression precipitate an aggressive neovascularization, which seems to be mediated by the activation of oncogenes and/or inactivation of tumor suppressor genes. Although the sequential order of specific genetic events in the malignant progression has not yet been fully understood, some genetic alterations might be directly linked to changes in the biosynthesis of angiogenic-related molecules. Recent studies involving experimental and human neoplasms have presented interesting results in terms of the interaction between genetic events and angiogenic growth factors. These include the finding that TSP1 production might be positively regulated by wild-type p53 in several cancers [1,7,8]. However, the relationship between TSP1 expression and the tumor suppressor gene in gliomas remains unclear [9]. Therefore, we studied the pathological significance of the alteration of wild-type *p53* and *p16* in the expression of TSP1 in order to ascertain whether these genetic events are responsible for the transformation of human gliomas into an angiogenic phenotype during the progression to malignancy.

2. Materials and methods

2.1. Recombinant adenovirus

Ad5CMVK-*p16*, a recombinant adenoviral vector, was constructed by following the previously published procedure [10]. The Ad5CMVK-*p16* contained the cytomegalovirus promoter, wild-type *p16* cDNA, which was obtained from Dr. D. Beach (Institute of Child Health, London) [11], as well as an SV40 polyadenylation signal in a minigene cassette, which was inserted into the E1-deleted region of the modified adenovirus 5.

The adenovirus, Ad5CMV-*p53* and Ad5CMV-*p21*, which contained the *p53* and *p21* gene, respectively, were kindly provided by Dr. Jack A. Roth (University of Texas, M.D. Anderson Cancer Center, TX).

2.2. Cell line and infection condition

The human glioma cell line U-251 MG, which was generously provided by Dr. N. Arita (University of Osaka, Osaka, Japan), was maintained in Dulbecco's modified Eagle's medium containing 10% heat-inactivated fetal bovine serum at 37 °C in a humidified atmosphere containing 5% CO_2. The *p53* gene is mutated (codon 273: CGT → CAT) [12], and the *p16* gene is endogenously deleted [13] in U-251 MG cells. Cell infection was carried out according to the previously described technique [14]. The culture medium was used for mock infection.

2.3. β-Galactosidase transduction assay

To assess the transduction efficiency of the adenoviral vectors, cells were infected for 36 h with Ad5CMV-*LacZ*, which carried the *Escherichia coli* β-galactosidase gene. Cells were stained with X-gal (5-bromo-4-chloro-3-indolyl-β-D-galactopyranoside; Sigma Chemical Co., St. Louis, MO). The percentages of β-gal-positive cells were determined on a plate reader (Inter Med, Tokyo) at a wavelength of 620 nm in each of three replicate dishes.

2.4. Cell growth curves

Cells were seeded at 2.5×10^4 cells/well in a 24-well plate. The cells were infected with either Ad5CMV-*LacZ* viral control, Ad5CMV-*p21*, Ad5CMV-*p53*, and Ad5CMVK-*p16*. Cultured medium alone was used for a mock infection control. Each sample was analyzed in triplicate. Cells were harvested and counted periodically until 60 h after the infection. Cell viability was determined by trypan

blue exclusion. The experiment was performed two times.

2.5. Flow cytometric assay

To analyze the DNA histogram, cell suspensions were prepared by trypsinization at 36 h after infection with Ad5CMV-*LacZ* viral control, Ad5CMV-*p21*, Ad5CMV-*p53*, and Ad5CMVK-*p16*. Cells were fixed with 70% ethanol and incubated with ribonuclease A (250 μg/ml; Sigma) for 1 h at 37 °C and propidium iodide (50 μg/ml; Sigma) for 10 min. Each sample was filtered through a 50-μm nylon mesh to obtain a single-cell nuclear suspension. They were analyzed on a FACSCalibur (Becton Dickinson, Mountain View, CA) with a minimum of 20 000 events for each sample. An argon laser at 488 nm excitation was used, and the samples were collected at 610 nm. ModFit LT (Becton Dickinson) was used for data analysis. Mean peak fluorescence was determined for each histogram. Three separate experiments were performed.

2.6. Western blot analysis

Cells were infected with medium alone, Ad5CMV-*LacZ* viral control, Ad5CMV-*p21*, Ad5CMV-*p53*, and Ad5CMVK-*p16*. Twenty-four (for p21, p53, and p16) and 36 (for TSP1) h after the infection, total cell lysates were prepared by lysing cell monolayers in plates with sodium dodecyl sulfate–polyacrylamide gel electrophoresis (SDS–PAGE) sample buffer (125 mM Tris–HCl, 2% SDS, 5% mercaptoethanol, 10% glycerine, pH 6.8) for 1 h at 4 °C after rinsing the cells with phosphate-buffered saline (PBS). Cell lysate protein (10 μg) from each sample was measured by BCA protein assay (Pierce, Rockford, IL) and subjected to 13.5% (for p21, p53, and p16) and 7.5% (for TSP1) SDS–Tris glycerine gel electrophoresis; it was then transferred to a PVDF membrane (Bio-Rad Laboratories, Hercules, CA). Membranes were blocked with 1% dry milk and 0.1% Tween-20 in Tris-buffered saline and incubated with the primary antibodies, mouse antihuman p21/WAF-1 monoclonal antibody (Oncogene Research Products, Cambridge, MA), mouse antihuman p53 monoclonal antibody (Dako Co., Carpinteria, CA), mouse antihuman p16 monoclonal antibody (Pharmingen, San Diego, CA), mouse antihuman TSP1 monoclonal antibody (Genzyme, Cambridge, MA), and mouse antihuman actin monoclonal antibody (Amersham Corp., Arlington Heights, IL). After rinsing in PBS, membranes were also incubated with a secondary antibody, horseradish peroxidase-conjugated sheep antimouse IgG (Amersham). The membranes were developed according to the Amersham enhanced chemiluminescence protocol.

2.7. Reverse transcription–polymerase chain reaction (RT–PCR) analysis

Cells (1.25×10^5) were infected with medium alone, Ad5CMV-*LacZ* viral control, Ad5CMV-*p21*, Ad5CMV-*p53*, and Ad5CMVK-*p16*. Total RNA was isolated from cultured cells using TRIZOL Reagent (Life Technologies Inc., Gaithersburg, MD) 24 h after infection. Total RNA sediment (400 ng) was reverse-transcribed in 50 mM Tris–HCl (pH 8.3), 75 mM KCl, 10 mM DTT, 3 mM $MgCl_2$, 0.5 mM dNTPs, and 0.2 μg of oligo$(dT)_{12-18}$ primer (Life Technologies) with 200 units of Moloney murine leukemia virus reverse transcriptase (Life Technologies) at 37 °C for 60 min. PCR was performed with human TSP1- and glyceraldehyde-3-phosphate dehydrogenase (GAPDH) (as an internal standard)-specific primers. Primers used were 5′-ACCGCATTCCA-GAGTCTGGC-3′ and 5′-ATGGGGACGTCCAACT-CAGC-3′ for TSP1 [15], and 5′-CAAAGTTGT-CATGGATGACC-3′ and 5′-CCATGGA-GAAGGCTGGGG-3′ for GAPDH [16]. Reverse transcription products (3 μl) were amplified by Taq DNA Polymerase (Promega Corp., Madison, WI) in 25 μl of a reaction mixture containing 5 mM Tris–HCl (pH 8.0), 10 mM NaCl, 10 μM EDTA, 0.1 mM DTT, 1.5 mM $MgCl_2$, 0.15 mM dNTPs, and 0.2 μM of TSP1 or GAPDH primers. Preliminary experiments showed that the amount of TSP1 and GAPDH cDNA PCR products reached a plateau after 28 and 32 cycles of reaction, respectively. Therefore, we amplified TSP1 cDNA under the condition of 24 cycles at 94 °C for 1 min, 60 °C for 1 min, and 72 °C for 2 min. Products were then electrophoresed on a 1% agarose gel. The intensity of the ethidium bromide luminescence was measured using a Fluor Imager SI (Amersham). The amount of TSP1 was normalized with that of GAPDH and expressed as relative to that

of the mock infection. The amplified 492 bp fragment of TSP1 cDNA was sequenced after being subcloned into pGEM-T Easy Vector (Promega). Three separate experiments were performed.

2.8. Northern blot analysis

Total RNA was extracted from the culture cells using TRIZOL Reagent (Life Technologies) 24 h after infection, while mRNA was isolated from the total RNA using Oligotex-dT30 (Takara, Tokyo, Japan). mRNA (3 μg) was fractionated on 1% denaturing formaldehyde/agarose gel and was transferred to Hybond-N membranes (Amersham) by capillary elution. Nylon filters were prehybridized at 42 °C for 2 h in a buffer containing 50% formamide, 4× SSC (20× SSC = 3.0 M NaCl and 0.3 M sodium citrate), 8× Denhardt's solution, and 0.2 mg/ml sheared denatured herring sperm DNA, hybridized with the ^{32}P-labeled TSP1 probe (500 000 cpm/ml buffer) at 42 °C overnight. A GAPDH probe was used as an internal control. Filters were washed at 42 °C in 2× SSC, 0.5% SDS, twice for 5 min and then once for 30 min in 0.1× SSC, 0.5% SDS. Autoradiography was then performed using a Bio-Imaging analyzer, FUJIX BAS 1000 (Fuji Photo Film Co. Ltd., Tokyo).

The amplified 492 bp fragment of TSP1 cDNA was used as a probe. The TSP1 cDNA probe was purified by 1% agarose gel electrophoresis, recovered with GENECLEAN III (BIO 101, La Jolla, CA), and radiolabeled with [α-^{32}P]dCTP (Amersham) using a DNA labeling kit (Amersham). Northern blots were repeated at least three times with RNA from different culture experiments.

2.9. Enzyme-linked immunosorbent assay

Cells (1.5×10^5) were plated on 12-well plates and grown for 24 h before viral infection. The cells were then infected with Ad5CMV-*LacZ* viral control, Ad5CMV-*p21*, Ad5CMV-*p53*, and Ad5CMVK-*p16*. Culture medium was used for mock infection. The medium was changed to G-5 Supplement (Life Technologies) containing Neurobasal Medium (Life Technologies) with medium alone, Ad5CMV-*LacZ*, Ad5CMV-*p21*, Ad5CMV-*p53*, and Ad5CMVK-*p16* after the cell monolayers were rinsed with PBS 24 h after infection. After 12 h, cell supernatants were collected and stored at −80 °C until use. The 96-well plates were coated with supernatants and serially diluted standard solutions (human thrombospondin; Athens Research and Technology Inc., Athens, GA) overnight at 4 °C. The plates were washed six times with PBS containing 0.05% Tween-20 (washing buffer) and blocked with 5% bovine serum albumin in PBS for 30 min at 37 °C. After the plates were washed, mouse antihuman TSP1 monoclonal antibody (Genzyme) was added, and the plates were incubated for 2 h at room temperature, then washed as above. Horseradish peroxidase-conjugated sheep anti-mouse IgG antibody (Amersham) and rabbit antigoat IgG secondary antibody (DAKO) were added and allowed to incubate for 3 h at room temperature. The plates were then washed six times with a washing buffer. Substrate solution (0.05% *o*-phenylenediamine dihydrochloride, 0.3% H_2O_2 in 0.1 M citric acid buffer) was added to the plates. After 10 min in darkness, the reaction was stopped by the addition of sulfuric acid. Absorbance at 490 nm was determined on a plate reader (Inter Med). Three separate experiments were performed.

2.10. Luciferase assay

A DNA fragment of TSP1 promoter and the first intron (−2040 to +750) were amplified by PCR and inserted into luciferase reporter vector pGL3-Basic, a promoter- and enhancerless vector (Promega). The sequence of the insert was confirmed by direct sequencing using a ABI PRISM 377 DNA sequencer (Perkin Elmer, Foster City, CA). Transfection of luciferase reporter plasmids was performed using DOTAP (Boehringer Mannheim), according to the protocol recommended by the manufacturer. Briefly, 1.0×10^4 cells seeded in 24-well plates were exposed to transfection mixtures containing 1.0 μg of luciferase reporter plasmids and 0.5 μg of pSV-β-galactosidase control vector (Promega). Then, the cells were harvested 48 h after the transfection. Luciferase assays were performed according to the manufacturer's protocols (Promega). β-Galactosidase assay was also performed with the same cell extracts in order to standardize for transcription efficiency. For p53 overexpression assay, 2.0 μg of p53 expression vectors were cotransfected with reporter plasmids, and luciferase assays were performed as described

above. As an effector control, the same amount of blank vector without p53 cDNA insert was used. All experiments were performed at least three times in each plasmid and represent the relative luciferase activity as average.

2.11. Statistics

All values are given as mean ± standard deviation. Student's *t* tests were used in all analyses.

3. Results

3.1. Influence of gene transduction on cell growth and exogenous gene products in U-251 MG cells

U-251 MG cells was infected with Ad5CMV-*LacZ* in the range of 0.39–400 multiplicity of infection (m.o.i.) in order to determine the adenoviral transduction efficiency as described previously. X-Gal staining showed that infection at an m.o.i. of 100 or greater was represented by 100% blue cells (Fig. 1). Infection with Ad5CMV-*p21* and Ad5CMVK-*p16* at an m.o.i. of 100 had no effect on the cell viability; however, infection with Ad5CMV-*p53* at an m.o.i of 100 decreased the viability due to apoptosis (data not shown). Therefore, Ad5CMV-*p21* and Ad5CMVK-*p16* at an m.o.i. of 100 and Ad5CMV-*p53* at an m.o.i. of 50 were used to maintain 100% viability in this study. This experimental condition demonstrated the fact that introduction of *p53*, *p16*, and *p21* did not suppress cell growth for 36 h after infection (Fig. 2A). As shown in Fig. 2B, U-251 MG cells accumulated in the G_0/G_1 phase at 36 h after infection with Ad5CMV-*p21*, Ad5CMV-*p53*, and Ad5CMVK-*p16* as compared with Ad5CMV-*LacZ*, and no significant difference was observed in the percentages of G_0/G_1 fraction among each introduced gene. The sub-G_0/G_1 fraction was not detected, indicating that apoptosis did not occur for 36 h after infection. Western blot analysis was performed in order to prove p21, p53, and p16 expression in virally transduced cells. Endogenous p21 was hardly detectable, and a high amount of mutant-type p53 was exhibited in U-251 MG cells. Endogenous p16 proteins were not detectable. On adenovirus-mediated gene transfer, exogenous p21, p53, and p16 were clearly demonstrated 24 h after infection with Ad5CMV-*p21*, Ad5CMV-*p53*, and Ad5CMVK-*p16*, respectively (Fig. 3). On this basis, we investigated the TSP1 expression within 36 h after adenoviral gene transfection of p21, p53, and p16 in order to exclude the possibility that the change in TSP1 expression was affected by growth inhibition induced by gene transduction.

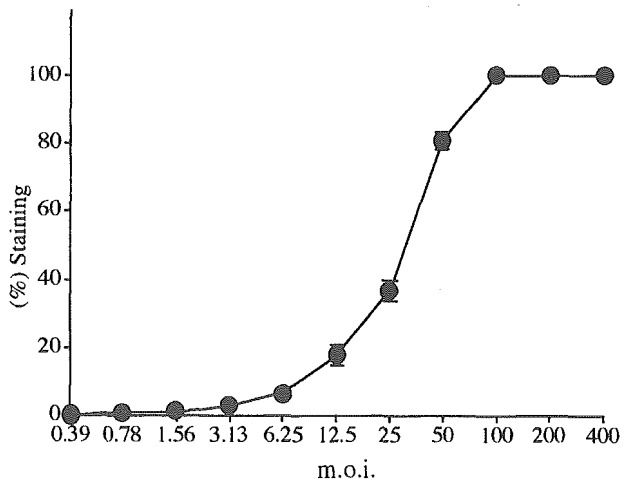

Fig. 1. Gene transduction efficiencies of U-251 MG cells. A recombinant β-gal adenovirus (Ad5CMV-*LacZ*) was used to infect the cells at different m.o.i. ranging from 0.39 to 400. The percentages of β-gal-positive cells were determined on a plate reader in each of three replicate dishes. Bars, standard deviation.

3.2. TSP1 expression is up-regulated by wild-type p53 transfection

RT–PCR was performed in order to detect TSP1 mRNA expression in virally transduced cells 24 h after infection (Fig. 4A). In U-251 MG cells, TSP1 mRNA expression in Ad5CMV-*p53*-treated cells was markedly up-regulated as compared with Ad5CMV-*LacZ*-treated cells. On the other hand, introduction of *p21* and *p16* had no effect on the TSP1 mRNA expression. In addition to RT–PCR, TSP1 mRNA expression was assessed by Northern blot analysis 24 h after infection. TSP1 mRNA expression in Ad5CMV-*p53*-treated U-251 MG cells was significantly increased as compared with that in Ad5CMV-*LacZ*-, Ad5CMV-*p21*-, and Ad5CMVK-*p16*-treated cells (Fig. 4B). These results were compatible with those of RT–PCR.

Western blot analysis demonstrated that TSP1 was

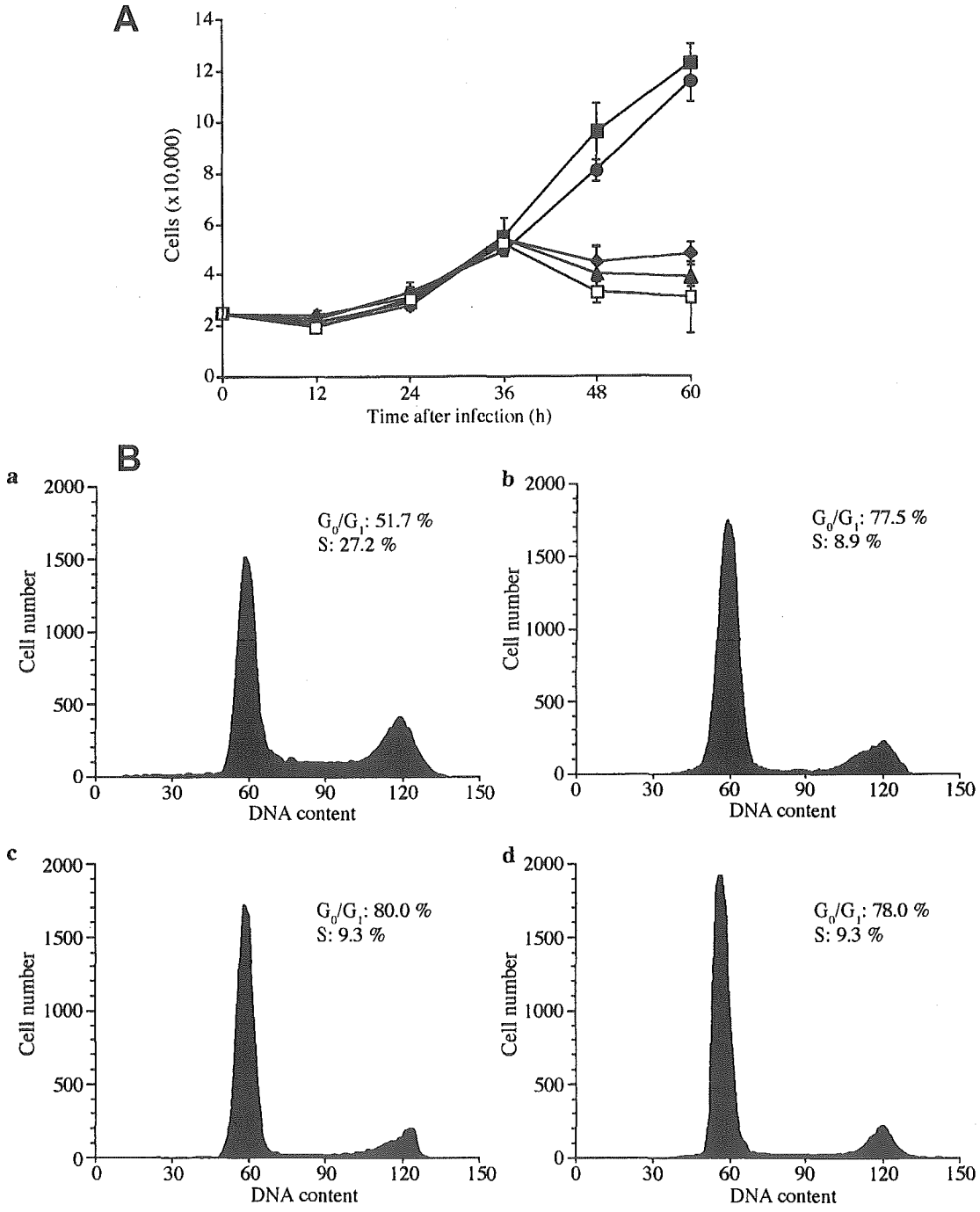

Fig. 2. (A) Growth curves of U-251 MG cells. Cells were plated at low-density (2.5×10^4) and infected with culture medium alone (■), Ad5CMV-*LacZ* (●), Ad5CMV-*p21* (▲), Ad5CMV-*p53* (◆), and Ad5CMVK-*p16* (□). Cell viability was assessed using the trypan blue exclusion test. The number of cells at each point is shown as the mean ± standard deviation of three different wells. (B) Effect of Ad5CMV-*p53*, Ad5CMV-*p21*, and Ad5CMVK-*p16* on cell cycle. U-251 MG cells were infected with Ad5CMV-*LacZ* (a), Ad5CMV-*p21* (b), Ad5CMV-*p53* (c), and Ad5CMVK-*p16* (d). Thirty-six hours after the infection, cells were analyzed for DNA content using flow cytometry.

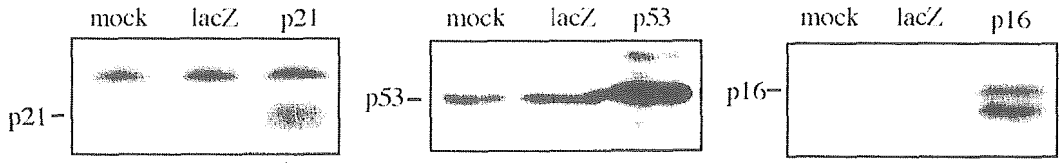

Fig. 3. Exogenous p21, p53, and p16 protein expressions in adenovirally transduced cells. U-251 MG cells were infected with medium only (mock), Ad5CMV-*LacZ* (lacZ), Ad5CMV-*p21* (p21), Ad5CMV-*p53* (p53), and Ad5CMVK-*p16* (p16). Cellular lysates were prepared 24 h after infection and subjected to Western blot analysis. Endogenous (mock infected) and exogenous (adenovirally infected) p21, p53, and p16 proteins were detected using monoclonal antibodies against p21, p53, and p16.

observed with an apparent molecular weight of 180 kDa (Fig. 5A). Induction of wild-type *p53* significantly increased TSP1 protein expression; however, TSP1 protein levels of Ad5CMV-*LacZ*-, Ad5CMV-*p21*-, and Ad5CMVK-*p16*-infected cells were not changed. Furthermore, the amount of TSP1 protein in a culture medium of cells transduced with adenoviral vectors was measured by enzyme-linked immunosorbent assay (ELISA) (Fig. 5B). Cell supernatants were collected 36 h after infection with Ad5CMV-*LacZ*, Ad5CMV-*p21*, Ad5CMV-*p53*, and Ad5CMVK-*p16*. TSP1 expression was not up-regulated by introduction of Ad5CMV-*p21* and Ad5CMVK-*p16*, but infection with Ad5CMV-*p53* increased TSP1 secretion 3.8-fold as compared with that caused by Ad5CMV-*LacZ* ($P < 0.001$).

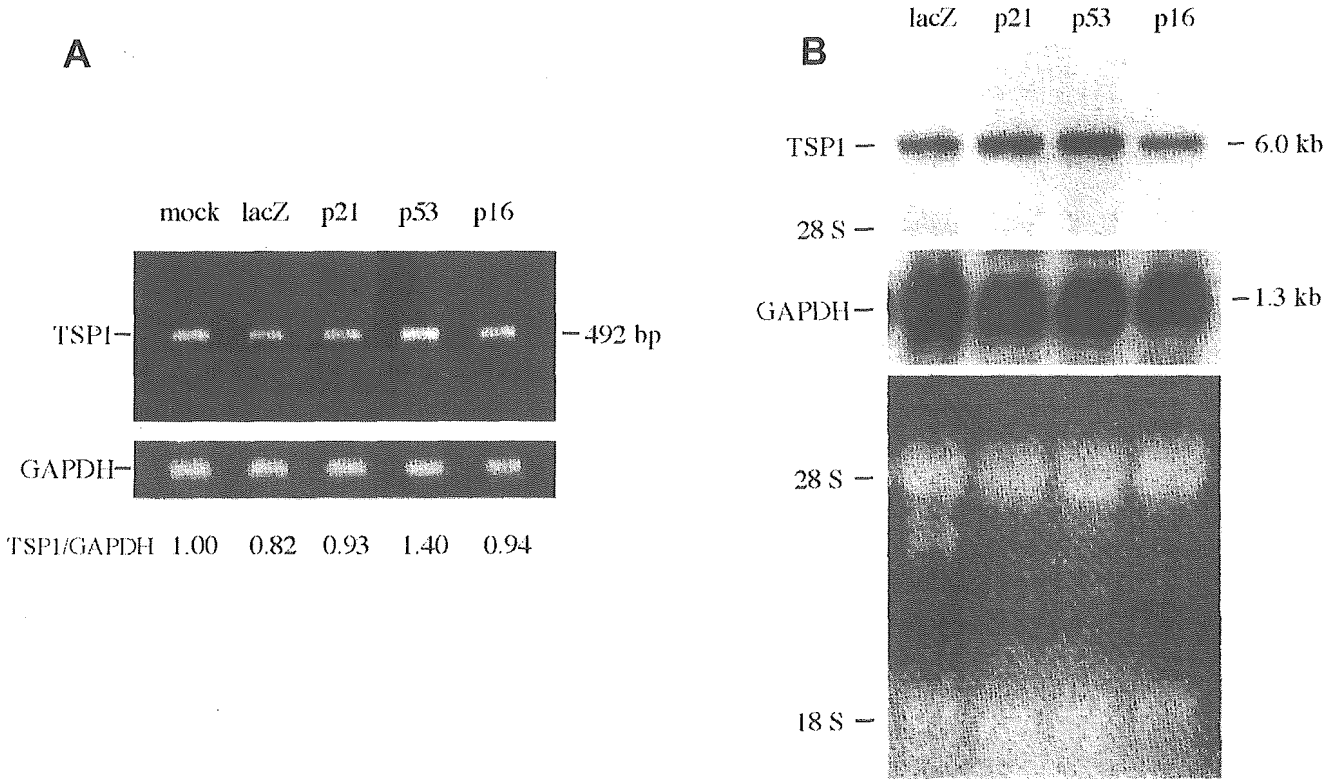

Fig. 4. Effect of Ad5CMV-*p21*, Ad5CMV-*p53*, and Ad5CMVK-*p16* on TSP1 RNA expression in U-251 MG cells. Cells were infected with medium alone (mock), Ad5CMV-*LacZ* (lacZ), Ad5CMV-*p21* (p21), Ad5CMV-*p53* (p53), and Ad5CMVK-*p16* (p16). (A) cDNA preparation of 492 bp corresponding to TSP1 was analyzed by RT–PCR. GAPDH transcripts were used as an internal control. PCR products were electrophoresed on 1% agarose gels and visualized by ethidium bromide staining. The amount of TSP1 expression was standardized with that of GAPDH and expressed as relative to that of the mock infection. (B) Northern blot analysis was performed in order to detect TSP1 RNA expression in U-251 MG cells. Upper panel, human TSP1 cDNA used as probe. Middle panel, human GAPDH cDNA was probed as an internal control. Lower panel, ethidium bromide-staining gel scanned at the 18S and 28S rRNA bands served as a loading standard.

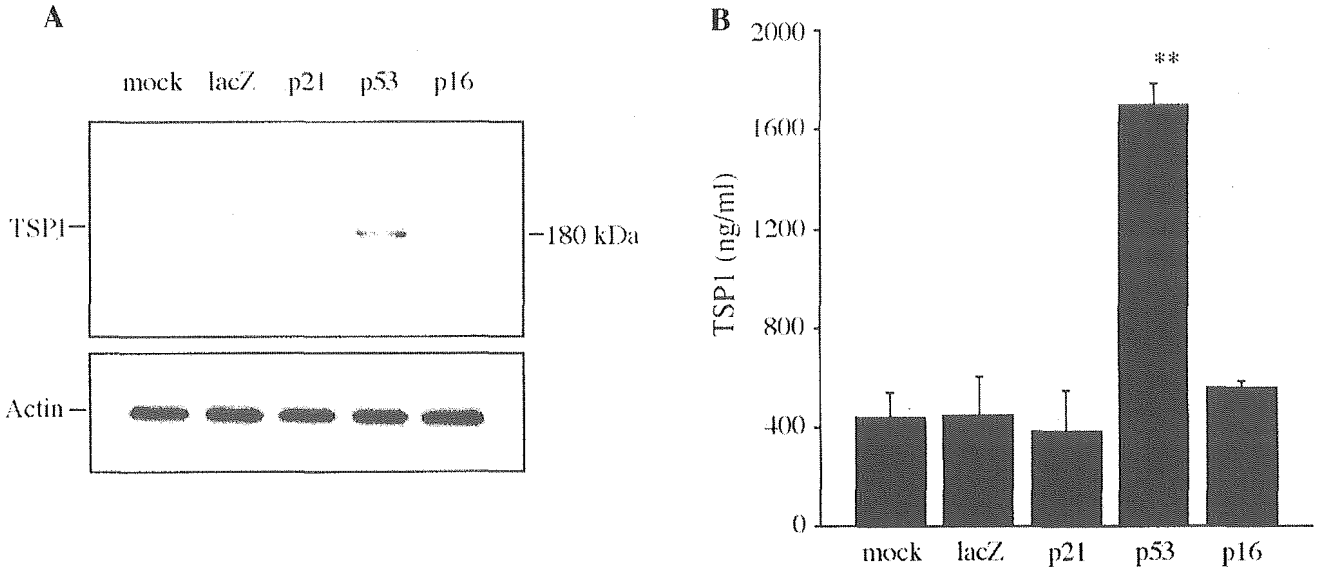

Fig. 5. (A) Detection of TSP1 protein in adenovirally transduced cells by Western blot analysis. U-251 MG cells were infected with medium only (mock), Ad5CMV-*LacZ* (lacZ), Ad5CMV-*p21* (p21), Ad5CMV-*p53* (p53), and Ad5CMVK-*p16* (p16). Cellular extracts were prepared 36 h after infection and subjected to Western blot analysis using monoclonal antibodies against human TSP1. Actin was probed as an internal control with monoclonal antibody. (B) Effect of wild-type *p21*, *p53*, and *p16* transfer on supernatant TSP1 protein levels in U-251 MG cells. Cells (1.5×10^5 cells) in triplicate wells were incubated on 12-well plates for 24 h in 10% fetal bovine serum-containing medium with medium alone, Ad5CMV-*LacZ*, Ad5CMV-*p21*, Ad5CMV-*p53*, and Ad5CMVK-*p16*. Each medium was changed for serum-free conditioned medium with medium alone (mock), Ad5CMV-*LacZ* (lacZ), Ad5CMV-*p21* (p21), Ad5CMV-*p53* (p53), and Ad5CMVK-*p16* (p16) and incubated for another 12 h. The supernatants were assayed by ELISA for TSP1. Values are means ± standard deviation of triplicate determinations. $^{**}P < 0.001$ versus mock, lacZ, p21, and p16.

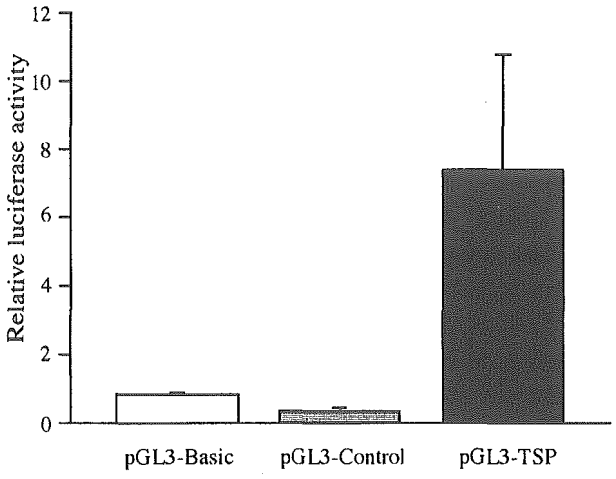

Fig. 6. Effects of wild-type p53 on transcription from the TSP1 promoter. U-251 MG cells were cotransfected with 2.0 μg of wild-type p53 expression vector or empty expression vector and 1.0 μg 2.8 kb TSP1 promoter construct (pGL3-TSP). pGL3-Basic without enhancer/promoter and pGL3-Control driven by SV40 enhancer/-promoter were used for control. The ordinate is relative luciferase activity determined versus activities in samples transfected with blank vector. Values are means ± standard deviation of triplicate determinations.

3.3. p53 enhances transcriptional activity of TSP1 promoter

To examine whether p53 regulates the promoter activity of TSP1, luciferase assays were performed using U-251 MG cells (Fig. 6). Expression of a reporter gene driven by the human TSP1 promoter (−2040 to +750) responded to the wild-type p53. In the presence of wild-type *p53* plasmid DNA, the promoter activity was increased 7.4-fold as compared with that of an empty expression vector control. Moreover, wild-type *p53* had no effect on the pGL3-Basic vector, the backbone luciferase plasmid into which the TSP1 promoter fragment was cloned, and the pGL3-Control vector, which has an SV40 promoter and enhancer.

4. Discussion

TSP1 has attracted attention as a possible negative regulator of tumor growth, metastasis, and angiogen-

esis based on its effect on tumor cells and endothelial cells. Although conflicting results have been reported regarding the function of TSP1 in tumor progression, increased TSP1 expression suppresses growth and metastasis and inhibits angiogenesis in some neoplasms [1]. The aim of this study was to investigate whether induction of wild-type *p53* or *p16* is associated with TSP1 production in gliomas. In the present study, we found that adenovirus-mediated wild-type *p53* transfer more significantly increased TSP1 mRNA and protein expression in the wild-type-*p53*-defective glioma cells (U251 MG) as compared with the reintroduction of wild-type *p16*. These findings indicate that p53 plays an important role in the regulation of TSP1 expression in wild-type-*p53*-inactivated glioma cells.

In Ad5CMV-*p21*-treated cells, no significant change in TSP1 expression was found. On the other hand, the degree of growth inhibition and cell cycle arrest was at the same levels among Ad5CMV-*p21*-, Ad5CMV-*p53*-, and Ad5CMVK-*p16*-treated cells. These findings suggest that TSP1 synthesis induced by wild-type *p53* is regulated by a different pathway, which is unrelated to control cell growth and cell cycle. Therefore, we performed luciferase assays in order to elucidate whether or not p53 might regulate the promoter activity of TSP1. Wild-type *p53* significantly enhanced the transcription of TSP1 promoter activity in U-251 MG cells. A recent study has indicated that the first intron contains two adjacent sequence elements that are similar to known p53 response elements and that wild-type *p53* regulates the TSP1 promoter (−2033 to +750) in cultured fibroblasts derived from Li-fraumeni patients [17]. In our study, p53 directly or indirectly up-regulated TSP1 mRNA expression at the transcriptional level.

The majority of tumors are angiogenic, and aberration of the genes may contribute to the transformation into an angiogenic phenotype following a change in the production of cytokines acting as angiogenic or antiangiogenic factors [18,19]. One of the most essential phenotypic changes that occur in tumorigenesis is the elimination of the normal cell's ability to product angiogenic inhibitors like TSP1 [20]. Although the correlation between *p53* alterations and TSP1 is controversial, some studies have indicated that TSP1 expression is regulated by p53 in several cancers [1,7–9,21]. In gliomas, p53 has been shown to control angiogenesis by modifying the production of an inhibitor, but the angiogenic inhibitor remains to be identified. Van Meir et al. [19] demonstrated the existence of glioma-derived angiogenesis inhibitory factor (GD-AIF), a physiological inhibitor of angiogenesis regulated by wild-type *p53* in glioblastoma cells. Nishimori et al. [22] have demonstrated that a candidate of GD-AIF is brain-specific angiogenesis inhibitor 1 (BAI1) identified as a *p53*-inducible gene product containing five thrombospondin-1 repeats predominantly recognized in the brain.

Recently, p53 has been found to play crucial roles in controlling tumor angiogenesis by regulating the expression of VEGF. Transfection of wild-type *p53* down-regulates VEGF expression and inhibits angiogenesis in colon carcinoma [23] and inhibits VEGF promoter activity in glioma cells [24]. Furthermore, we have previously shown that the wild-type *p53* and *p16* down-regulate VEGF expression and inhibit angiogenesis in human gliomas [25]. In particular, wild-type *p16* transfer reduced VEGF expression more potently than did wild-type *p53* transfer. The mechanisms leading to the alteration of the balance between the inducers and inhibitors of neovascularization are not well known. It is generally considered that some gliomas become potently angiogenic founded on the inactivation of *p53* and *p16*. We speculate that the mutation of *p53* results in a significant decrease in the secretion of TSP1 and an increase in the secretion of VEGF and that it promotes angiogenesis. The loss of the *p16* tumor suppressor gene, which results in a further up-regulation of VEGF secretion, is involved in the progression of the angiogenic phenotype. The aberrations of the *RB* gene and *PTEN* on chromosome 10q, which are detected in a majority of high-grade gliomas may also have an influence on angiogenesis [26], however, alterations of *p53* and *p16* may be necessary in order for gliomas to progress to full malignancy with hyper-vascularization.

Gliomas resist all current treatments including surgery, radiotherapy, and chemotherapy, so that a therapeutic breakthrough requires the development of new concepts and new target molecules. The most current approach aims to establish a gene therapy designed to reintroduce tumor suppressor genes. The present study and more recent data disclose the fact